Onset of Turbulence and Profile Resilience in the Helimak Configuration

K. Rypdal
Department of Physics, University of Tromsø, 9037 Tromsø, Norway

S. Ratynskaia
Max-Planck-Institute for Extraterrestrial Physics, Postfach 1312, D-85740 Garching, Germany
(Received 30 December 2004; published 7 June 2005)

An experimental study of the onset of drift wave and flute interchange instabilities in the Helimak configuration is presented. It is shown that the Helimak offers the opportunity to separate the regions where these instabilities are active and to assess their relative role in cross-field anomalous transport and in the self-organization of exponential plasma density profiles with resilient scale length. Some results indicating a period doubling route to turbulence are also presented.

DOI: 10.1103/PhysRevLett.94.225002 PACS numbers: 52.25.Xz, 52.25.Gj, 52.35.Kt, 52.35.Py

The Helimak is the simplest toroidal plasma configuration that permits a magnetohydrodynamic equilibrium [1] and is a promising tool for the experimental study of magnetic plasma confinement. Recently, the configuration has attracted considerable interest in the magnetic fusion community and has led to the construction of a new generation of medium size magnetic confinement devices [1,2]. The Helimak is very suitable for studies of low-frequency gradient driven instabilities and their routes to turbulence in the presence of magnetic field curvature and shear, and, related to this, cross-field turbulent transport and formation of universal plasma profiles. Yet, so far little has been published on these subjects from the Helimak configuration since the paper of Zimmerman and Luckhardt in 1993 [3], and this Letter presents the first systematic study in this direction.

The Helimak configuration consists of a purely toroidal magnetic field B_φ with a weak vertical magnetic field component B_z superposed, and the key parameter is the magnetic pitch ratio $r_B = |B_z|/B \sim 10^{-2}$, where $B = (B_\varphi^2 + B_z^2)^{1/2}$. It is convenient to introduce cylindrical coordinates (r, φ, z), where $r = R - R_0$ denotes the distance along the major radius from the minor axis, z is the distance from the horizontal midplane in the direction along the major torus axis, and φ is the toroidal angle. The helical field lines ascend a vertical distance $\Delta z_B \approx 2\pi R r_B$ between two successive intersections with the poloidal plane $\varphi = 0$. If the plasma is weakly ionized, the perpendicular electric conductivity $\sigma_\perp = m_i n \nu_{in}/B^2$ is determined by the perpendicular ion mobility due to ion-neutral collisions, and the parallel conductivity $\sigma_\parallel = e^2 n/(m_e \nu_{en})$ by the electron mobility. Because of the magnetic pitch, the vertical conductivity is given as $\sigma_z \approx \sigma_\parallel r_B^2 + \sigma_\perp$, while the radial conductivity is $\sigma_r = \sigma_\perp$. The equipotential surfaces are elongated in the z direction into a slablike structure if $(\sigma_\parallel/\sigma_\perp) r_B^2 = (\Omega_e/\nu_{en}) \times (\Omega_i/\nu_{in}) r_B^2 \gg 1$, and the equipotential surfaces may be almost vertical.

The experiment reported in this Letter is performed in a hot filament cathode discharge in the "Blaamann" torus [4], which has major radius $R_0 = 65$ cm and minor radius $a = 13$ cm. Figure 1 shows contours of the time-averaged plasma potential ϕ and electron pressure $p = n_e T_e$ as measured by the floating potential of a "plug probe" and the electron saturation current of a conventional cylindrical Langmuir probe [5] in a Helimak discharge with helium gas pressure 0.35 Pa, $B = 18$ mT, $B_\varphi > 0$, $B_z < 0$, and $r_B = 0.01$. The plug probe is a field-aligned cylindrical Langmuir probe equipped with ceramic end plugs to reduce the electron saturation current. Such a probe has been shown to float close to the plasma potential [5]. The other details of the experimental setup and the diagnostics are the same as in Ref. [4].

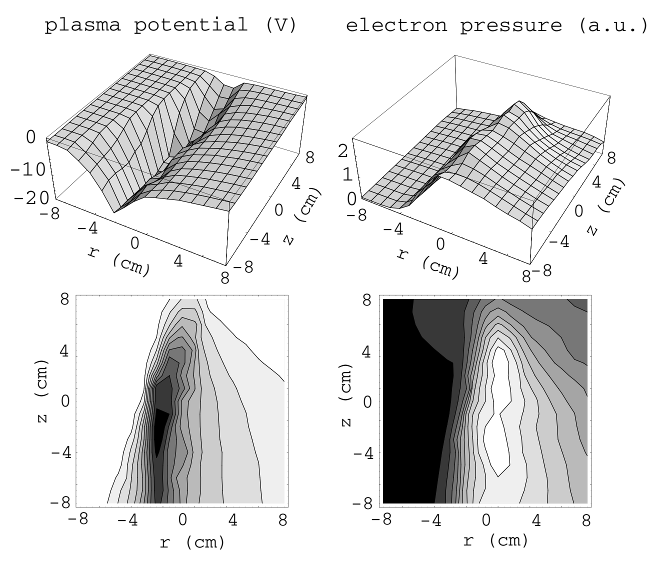

FIG. 1. Time-averaged quantities in a poloidal cross section for $B = 18$ mT. Left column: Plasma potential. Right column: Electron pressure.

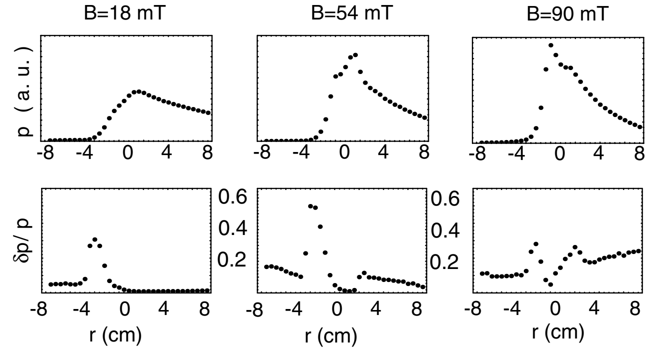

FIG. 2. Radial profiles of time-averaged electron pressure p_0 (upper row) and standard deviation of relative electron pressure fluctuations $\delta p/p = \langle(\tilde{p} - p_0)^2\rangle^{1/2}/p$ (lower row) for three different values of magnetic field B. Profiles are measured in vertical position $z = -4$ cm. The vertical scale of the figures in the upper row are in the same arbitrary units.

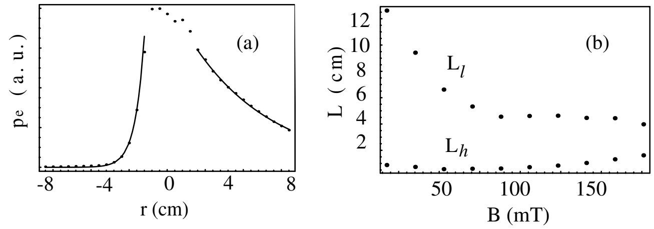

FIG. 3. (a) Exponential fits to electron pressure profile for $B = 72$ mT. (b) Lower curve shows variation of scale length L_h with magnetic field B as obtained from fitting the function $c_h \exp(r/L_h)$ to the profile. Upper curve shows the dependence of L_l from fitting the function $c_l \exp(-r/L_l)$ to the profile.

At this weak magnetic field the plasma is very quiet and the particle transport is dominated by stationary $\mathbf{E} \times \mathbf{B}$ convection. The plasma source is an electron emitting tungsten wire stretched vertically along the bottom of the potential "canyon," and the plasma flow follows the equipotentials upwards on the high field side (HFS) of the density maximum and downwards on the low field side (LFS). The left-right asymmetry of these contours with respect to a vertical line at $r = 0$ can be explained as follows: Ionization occurs mainly at a vertical strip near $r = 0$ and the plasma is convected towards the LFS, explaining the steep density gradient on the HFS. Charge emitted from the filament is neutralized by a field-aligned electron current driven by a weak E_z component and a radial ion current driven by the strong E_r component. Both mechanisms require a negative plasma potential in the filament region, and since the negative charge will be convected with the plasma flow, there will also be a negative potential on the LFS. The up-down asymmetry is due to a downwards directed E_z arising from the vertical curvature and gradient drifts. This field is superposed on E_r, resulting in a "fan" of potential contours that open towards the lower LFS, allowing the plasma to flow to the wall in this region.

When the magnetic field strength B is increased (while keeping constant pitch $r_B = 0.01$), E_z is reduced, and so is the spread of the fan of potential contours. This results in a steeper electron pressure gradient on the LFS, and at $B = B_T \approx 50$ mT there is a sudden onset of fluctuations on the LFS. The radial electron pressure profile $p(r)$ and the root-mean-square of the normalized electron pressure fluctuations are shown in Fig. 2 for magnetic fields below and above threshold. For the lower field the pressure scale length on the HFS is less than 1 cm, and there are some weak fluctuations located to the steep gradient in this region. On the LFS the scale length is 13 cm, and the fluctuations are of the same level as the instrumental noise. With increasing B the profiles on both sides are exponential, the gradients grow steeper [see Fig. 3(b)], and the fluctuation level on the HFS increases (Fig. 2). Above threshold, fluctuations are also excited on the LFS, but it is observed that they are confined to the regions of steep pressure gradients on both sides of the pressure maximum. For $B \gg B_T$, fluctuations on the LFS are much stronger than on the HFS. On the LFS the threshold scale length is $L_l \approx 6$ cm, and the gradient continues to steepen somewhat until $L_l \approx 4.5$ cm at $B = 80$ mT (see the caption of Fig. 3 for the precise definition of L_l and L_h). For higher magnetic fields than this, L_l remains approximately constant. On the HFS there is a slow increase in the scale length L_h above threshold due to a gradual penetration of plasma into the region to the left of the pressure maximum.

The power of the fluctuations on the LFS just above threshold resides mostly in a narrow peak around 12 kHz, as depicted in Fig. 4(a). The total power in the fluctuations continues to increase until $B \approx 80$ mT, after which it remains nearly constant. The saturation of the fluctuation power, and the establishment of a resilient profile with constant L_l, is associated with a period doubling succeeded by growth of a broad turbulent spectrum at low frequen-

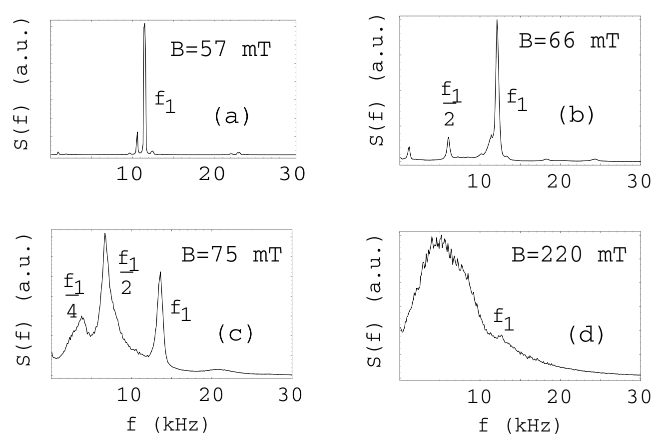

FIG. 4. Power spectra for electron pressure fluctuations on the LFS ($r = 4$ cm, $z = -4$ cm) for increasing magnetic field.

cies. This evolution of the spectrum with increasing B is shown in Fig. 4.

The nature of the fluctuations is studied by locating a reference probe at the position $r = 4$ cm, $\varphi = 120°$, and by moving another probe vertically in the plane $r = 4$ cm, $\varphi = 0°$ in the interval $z = -8$ cm to $z = 8$ cm in steps of 0.5 cm. In every location 1×10^6 samples of electron pressure fluctuations are recorded simultaneously from both probes at a sampling frequency of 100 kHz, and frequency spectra of cross coherence $\gamma(f)$ and cross phase $\alpha(f)$ between the two signals are estimated (see Ref. [5] for details). Cross coherence and cross phase for frequencies 3.5, 14, and 28 kHz versus vertical position z of the moving probe are depicted in Fig. 5 for $B = 75$ mT. The power spectrum in Fig. 4(c) shows a prominent primary peak at $f = f_1 \approx 14$ kHz, an even stronger peak at the subharmonic $f = f_1/2 \approx 7$ kHz, and an additional bump peaking near $f = f_1/4 \approx 3.5$ kHz. In Fig. 6 the same quantities are plotted for $f = 5$, 10, 15 kHz and $B = 220$ mT, when a broad turbulent spectrum has developed [Fig. 4(d)]. Local maxima of the cross coherence occur when the two probes (which are separated 120° toroidally) are located on the same field line. Except for Fig. 6(d), these maxima coincide with the location of zero cross phase, indicating that the fluctuations are associated with modes strictly elongated along the helical field lines (flute modes). Whenever the primary peak at f_1 is clearly visible in the spectrum the coherence and cross phase looks like Figs. 5(b) and 5(e). This shows that the wave at f_1 is a flute mode which does not lose significant coherence as one follows a field line one turn around the torus. The Δz for which the cross phase varies by 2π could be interpreted as the vertical wavelength at this frequency, and we observe that $\lambda_z = 2\pi/k_z = \Delta z_B$. The sharp frequency peak at f_1 observed for B just above B_T corresponds to the solution of a linear dispersion relation for the flute mode in the laboratory frame of reference (roughly $f_1 \approx v_{Ez}/\lambda_z$, where v_{Ez} is the z component of the $\mathbf{E} \times \mathbf{B}$ velocity on the LFS). For $f \neq f_1$ there is typically a coherence loss along the field lines, and associated with this is a statistical spread of the cross phase when this quantity is estimated over a large number of subrecords. Nevertheless, the *averaged* cross phase shown in Figs. 5(d), 6(e), and 6(f) has the same spatial dependence as for $f = f_1$, indicating a locking of the average wavelength to Δz_B over a broad range of frequencies. Figures 5(c), 5(f), 6(a), and 6(d), however, exhibit exceptions to this rule, whose main features can be explained by the following model.

Let us assume that the time Fourier transform of the total wave field at a given radial location r can be written in the form $\psi(z, \varphi, \omega) = A(\omega)\exp[i(k_z z + \varphi)] + B(\omega) \times \exp[i(K_z z + n\varphi)]$, where $A(\omega)$ and $B(\omega)$ are statistically independent so that $\langle A(\omega)B^*(\omega)\rangle = 0$. The first term with amplitude $A(\omega)$ represents a quasicoherent flute mode with vertical wave number $k_z = 2\pi/\Delta z_B = 1/Rr_B$. For the second term with amplitude $B(\omega)$, we shall consider two different cases. If $K_z = 2k_z$ and $n = 2$, this term represents a flute mode of half the wavelength of the primary mode (second wave-number harmonic). Since a quasicoherent flute mode field will have to satisfy the periodicity condition $\psi(z + \Delta z_B, \varphi, \omega) = \psi(z, \varphi, \omega)$, a more general form of the wave field would be Fourier series containing all higher wave-number harmonics, but inclusion of a second harmonic is sufficient to explain the behavior in Fig. 5(f). In Figs. 7(a) and 7(d) we show the coherence and cross phase calculated from this model with $\mu \equiv |B(\omega)/A(\omega)| = 1/2$. Since this model assumes a superposition of two coherent modes, it cannot describe the coherence loss along field lines, but otherwise it reproduces the behavior of Figs. 5(a), 5(d), 6(b), 6(e), 6(c), and 6(f). Thus, the spatial oscillations of the coherence can be explained by the presence of a second wave-number harmonic of amplitude weaker than the primary mode. As $\mu \rightarrow 1$ the amplitude of these oscillations grows until the coherence oscillates between 0 and 1 when $\mu = 1$. For $\mu > 1$ this amplitude is again reduced, but now the second harmonic

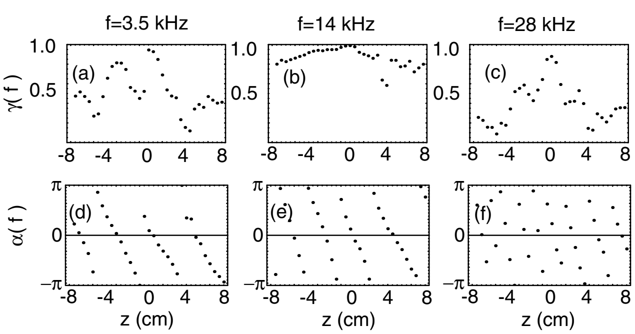

FIG. 5. Cross coherence $\gamma(f)$ and cross phase $\alpha(f)$ of electron pressure fluctuations for $B = 75$ mT, and $f = f_1/4 \approx 3.5$ kHz, $f = f_1 \approx 14$ kHz, $f = 2f_1 \approx 28$ kHz as a function of vertical position of moving probe. The plots for $f = f_1/2 \approx 7$ kHz are very similar to those for $f = f_1/4$. Reference probe located on the LFS at position $\varphi = 120°$, $r = 4$ cm, $z = 0$ cm. Moving probe scanning along a vertical line at $\varphi = 0$, $r = 4$ cm in steps of 0.5 cm in the range $z = (-8, 8)$ cm.

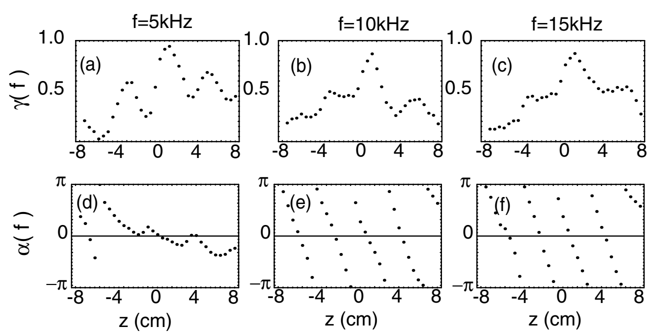

FIG. 6. Same as Fig. 5, but with $B = 220$ mT and for frequencies $f = 5$, 10, 15 kHz.

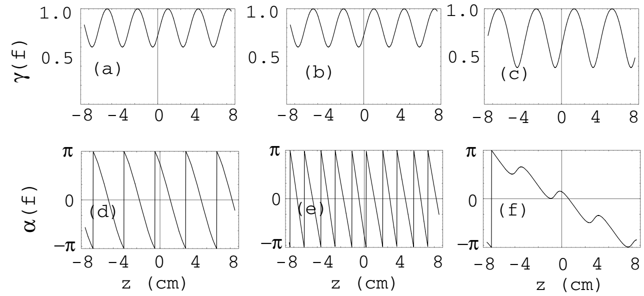

FIG. 7. Theoretical estimates of cross coherence $\gamma(f)$ and cross phase $\alpha(f)$ for $\lambda_z = 3.3$ cm. (a),(d) Second mode is second harmonic flute mode and $\mu = 1/2$. (b),(e) Second mode is second harmonic flute mode and $\mu = 2$. (c),(f) Second mode is toroidal drift mode with $n = 0$, $\Lambda_z = 16$ cm, and $\mu = 2$.

becomes apparent in the cross-phase variation and the situation looks like Figs. 7(b) and 7(e) for $\mu = 2$, which qualitatively reproduces the experimental result depicted in Figs. 5(c) and 5(f). These results indicate that for $B = 75$ mT the field is composed of flute modes where the wave-number spectrum is dominated by the primary wave number k_z and its second harmonic, and where the primary wave number dominates for $f \leq f_1$ and the second harmonic dominates at higher frequencies.

The behavior at $B = 220$ mT can be explained by assuming that the second mode is a toroidal drift mode of vertical wave number $K_z \ll k_z$ and toroidal mode number $n = 0$. Figures 7(c) and 7(f) depict the resulting coherence and cross phase for $\lambda_z = 2\pi/k_z = 3.3$ cm, $\Lambda_z = 2\pi/K_z = 16$ cm, and $\mu = 2$, which conforms quite well with the experimental results shown in Figs. 6(a) and 6(d). Also in this case the coherence oscillation attain amplitude of unity when $\mu \to 1$, and for $\mu < 1$ the graphs look similar to those depicted in Figs. 7(a) and 7(d). The cross phase for plasma potential fluctuations for $f = 5$ kHz does not exhibit the behavior depicted in Fig. 6(d), but rather looks like Figs. 6(e) and 6(f). This is reasonable since the potential amplitude relative to the density amplitude is considerably smaller for drift waves than for flute modes. Thus we conclude that for fully developed turbulence at $B = 220$ mT we have low-frequency ($f \leq 5$ kHz) toroidal drift modes of somewhat higher amplitudes coexisting with flute modes. At higher frequencies, we infer that drift modes (or maybe second harmonic wave-number flute modes) of somewhat weaker amplitude may coexist with primary wave-number flute modes.

Measurements similar to those presented in Fig. 5 have also been performed by locating the reference probe on the HFS at $r = -4$ cm, and moving the other probe vertically at this radial position. Spectra are generally different from what is observed on the LFS, and fluctuations in these two regions are almost uncorrelated. Maximum cross coherence and zero cross phase is now obtained when the two probes are in the same poloidal position, and not when they are located on the same field line. Moreover, rather than observing locking of the wavelength to Δz_B, the perpendicular wave number satisfies a linear dispersion relation. The wavelengths at $f = 5$, 10, and 15 kHz are 18, 9, and 6 cm, respectively, and agree well with the wavelength of 16 cm found for the drift wave at 5 kHz inferred from Figs. 6(d) and 7(f) for fluctuations on the LFS. These observations are all consistent with a spectrum of drift modes with toroidal mode number $n = 0$. The absence of flute modes is not surprising, since these modes are not unstable on the HFS.

The evolution of the power spectrum shown in Fig. 4 could indicate a period doubling sequence and a Feigenbaum route to chaos [6]. However, spectral broadening appears already when the first period doubling bifurcation occurs, and it is impossible to follow the cascade beyond the second period doubling. The locking of the flute mode wave number to a single mode indicates that the wave field can be represented by a low dimensional set of autonomous ordinary differential equations. A complicating factor, however, is the excitation of drift waves, whose wave numbers are not locked. The nonlinear interaction of flute modes with this continuous spectrum of drift waves may be the cause of the observed spectral broadening.

This Letter has presented a study of the onset of drift wave and flute interchange instabilities in the Helimak. Using the magnetic field strength as a control parameter, it was demonstrated that there is a threshold B_T for electrostatic flute modes ($k_\parallel = 0$) on the low B-field side of density maximum. For $B > B_T$ radial profiles of electron pressure are exponential on both sides, but on the low field side the scale length approaches a constant value as B is increased. The formation of this resilient profile occurs as power spectra of electrostatic fluctuations evolve from single frequency at threshold, via a period doubling route to turbulence when $B \gg B_T$. In the turbulent-resilient state, flute modes and drift waves coexist on the low field side, while only weak fluctuations of drift wave type are observed on the high field side.

[1] S. H. Müller, A. Fasoli, B. Labit, M. McGrath, M. Podestà, and F. M. Poli, Phys. Rev. Lett. **93**, 165003 (2004).

[2] K. Gentle, W. Rowan, and S. Luckhardt, Bull. Am. Phys. Soc. 48 (2003), poster LP1 74.

[3] E. D. Zimmerman and S. C. Luckhardt, J. Fusion Energy **12**, 289 (1993).

[4] K. Rypdal and S. Ratynskaia, Phys. Plasmas **11**, 4623 (2004).

[5] S. Ratynskaia, V. Demidov, and K. Rypdal, Phys. Rev. E **65**, 066403 (2002).

[6] D. Ruelle, *Chaotic Evolution and Strange Attractors* (Cambridge University Press, Cambridge, 1989).